MAPPING OF SMALL WATER BODIES WITH INTEGRATED SPATIAL INFORMATION FOR TIME SERIES IMAGES OF OPTICAL REMOTE SENSING

Libei Fan [1], Yuting Dong [1,], Ji Zhao [2], Christian Geiß [3], Lizhe Wang [2], Hannes Taubenböck [3,4]*

[1]School of Geography and Information Engineering, China University of Geosciences, Wuhan, China
[2]School of Computer Science, China University of Geosciences, Wuhan, China
[3]German Aerospace Center (DLR), German Remote Sensing Data Center (DFD), Oberpfaffenhofen 82234, Germany
[4]Institute for Geography and Geology, Julius-Maximilians-Universität Würzburg, Würzburg 97074, Germany
*Corresponding author: dongyt@cug.edu.cn

IGARSS 2022 - 2022 IEEE International Geoscience and Remote Sensing Symposium | 978-1-6654-2792-0/22/$31.00 ©2022 IEEE | DOI: 10.1109/IGARSS46834.2022.9883460

ABSTRACT

Small water bodies and their temporal changes are, especially in urban areas, closely related to the urban climate, people's daily life, among others. Mapping of small water bodies with optical remote sensing images in complex urban landscapes is challenging: that is to establish a balance between reducing incorrect water detection and increasing the integrity of water extraction. In this work we propose a spatial information-integrated small water bodies mapping (SWM) method to achieve a complete and accurate extraction and temporal change monitoring of small water bodies. The spatial contextual information is exploited by the proposed water index roughness feature to compensate for the indistinguishability of small water bodies in spectral information. Results using Landsat and Sentinel-2 data show that the proposed algorithm achieves better water extraction performance, i.e. higher completeness and less incorrect extractions. It proves the ability to observe the changes of surface water.

Index Terms— Small water bodies mapping, Water index, Sentinel-2, Landsat, Spatial information

1. INTRODUCTION

Small water bodies, including ponds and small lakes, low-order streams, ditches and springs, are undergoing temporal and spatial changes given the changes in land use/cover [1] and various environmental changes in the process of urbanization [2]. These may lead to negative effects concerning the urban climate or recreation, or even to disasters that endanger the safety of life and property, such as floods and water shortages. Therefore, monitoring small water bodies for a better understanding of its local-specific effects is essential for better informed urban planning decisions.

Small water bodies with limited size and of large numbers pose significant challenges for high-precision mapping. As the availability of high spatial resolution optical satellites (such as Landsat and Sentinel-2 multispectral satellites) increases, rapid and accurate surface water extraction and mapping using optical remote sensing technology has been widely used in various water-related applications [e.g., 3]. The water extraction method based on spectral analysis is realized by thresholding the water index image and has been widely used. And, by enhancing the contrast between water bodies and other land covers relatively high performance measures have been achieved [4].

The accuracy for mapping water bodies using water index approaches depends on the selection of threshold. The threshold can be set empirically or automatically. As one of the most used algorithms, the Otsu algorithm obtains optical thresholds by maximizing the variance between water bodies and other land covers [5]. However, the variability of spectral information within and across satellite data brings challenges to setting appropriate transferable thresholds as settings are often specific to each study case [6]. Specifically, shadows as example often have a water index value similar to or higher than the water body itself, which may create several false positives (incorrect extractions). To reduce false positives, the threshold to segment the water index map may need to be set relatively high (closer to value 1). On the other hand, small water bodies tend to have relatively small water index values compared to pure water bodies, due to the influence of the surrounding environment and mixed pixels. To completely extract small surface water bodies, it is best to set the corresponding threshold value lower (closer to -1). It is thus challenging to adjust the threshold to reduce incorrect water extractions and increase the precision of detected water bodies at the same time. In addition, it is especially important and difficult to determine the optimal threshold for time-series analysis of water bodies. Changes in the state of the water bodies will affect their corresponding spectral albedo. Different atmospheric conditions, angles of incidence of sunlight, or radiometric calibration states of time-series remote sensing images

acquired by different sensors also cause variation in the image radiation values.

To overcome the instability of spectral information and to achieve sufficient, accurate observations of long-term surface water dynamics of the small water bodies, we propose a spatial information-integrated small water bodies mapping algorithm (SWM) for time-series of Landsat and Sentinel-2 optical remote sensing imagery. In the SWM algorithm, the spatial contextual information is exploited to compensate for the uncertainty of spectral information and to refine and extract small water bodies from multiple perspectives of feature mining and decision-making.

2. METHODOLOGY

The SWM algorithm consists of the following three steps: Firstly, the probabilistic categories 'certainly water surfaces' and 'potentially water surfaces' are identified by hierarchically dividing the water body index. Secondly, the water index roughness and SWIR band are used to refine both categories by analyzing the 'potentially water' pixels in the initial step. Finally, the obtained 'certainly water' and 'potentially water' are spatially merged to achieve an accurate surface water map. The details of the proposed SWM algorithm are given in the following three sections.

2.1. Identifying the thematic classes 'potentially water' and 'certainly water'

Generally, most pure water pixels have higher water index values and exhibit relatively large differences to non-water pixels in all water indexes. However, it is difficult to extract some water bodies of very small sizes, such as small lakes or ponds and narrow rivers, due to the small difference in the water index between them and non-water materials. To extract these water bodies at these small scales, we consider the pure water pixels as 'certainly water' (C1) and a pixel that potentially shows a water surface as 'potentially water' (P1). They can be obtained based on the Eq. (1) and Eq. (2).

$$C1 = \{i \in V \mid WI_i > T_{pure}\} \tag{1}$$

$$P1 = \{i \in V \mid T_{mixed} < WI_i \le T_{pure}\} \tag{2}$$

where V is a set of pixels. T_{pure} and T_{mixed} are respectively the high threshold and the low threshold, which can be automatically calculated based on Eq. (3) and Eq. (4).

$$T_{pure} = \max\left\{T_s, 0.5\times\left(M_1 + std_1\right)\right\} \tag{3}$$

$$T_{mixed} = \min\left\{T_s, 0.5\times(M_2 - std_2)\right\} \tag{4}$$

where T_s is the initial threshold of the water index, which can be obtained by experience or by automatic threshold determination by the Otsu approach. Based on the threshold T_s, the water index can be divided into two parts as a whole. One part is a water index greater than the threshold T_s, which contains most of the water bodies. The median and variance of this part of the water index can be calculated and expressed as M_1 and std_1 as shown in Eq. (3). The other part is a water index less than or equal to the threshold T_s, and is mainly composed of non-water land cover types. Their corresponding median and variance can be expressed as M_2 and std_2 shown in Eq. (4).

2.2. Refining the thematic classes 'potentially water' and 'certainly water'

To reduce the false positives and improve the accuracy of small water bodies, the initial thematic classes 'potentially water' and 'certainly water' need to be further refined. Firstly, the SWIR band is used to prune non-water land cover types in the category 'potentially water'. The collection of new pixels of 'potentially water' after removing non-water materials is denoted as P2, and can be defined as:

$$P2 = \left\{i \in P1 \middle| \rho_{SWIR,i} < T_{SWIR}\right\} \tag{5}$$

where pixel i belongs to P1, and $\rho_{SWIR,i}$ is the SWIR band reflectance of pixel i. T_{SWIR} is a specified experience threshold and can be set to be 0.1.

On the other hand, we refine the category 'certainly water' by expanding the spatial distribution of these pixels from 'potentially water' P2 to avoid missing water bodies. We propose the water index roughness (WIR) and use the spatial variability of the water index to extract pixels of 'certainly water' in the already assigned 'potentially water' areas, which can be computed as follows:

$$WIR_i = \max_{j\in N_i}\left\{WI_j\right\} - WI_i \tag{6}$$

where N_i is the local neighborhood of pixel i, and a window of size 5 is used to represent the neighborhood in this study. WI_i is the water index value of pixel i. The new pixels of category 'certainly water' are denoted as C2 and can be defined as:

$$C2 = \left\{\left\{C1, i \in P2\right\} \middle| WIR_i > T_{WIR}\right\} \tag{7}$$

where pixel i belongs to P2, and WIR_i is the water index roughness of pixel i. T_{WIR} is the specified threshold and is empirically set to 0.4 in this study. The category 'potentially water P2', if the WIR value of a pixel is greater than the threshold T_{WIR}, is classified into the category 'certainly water'.

2.3. Mapping multi-scale water based on spatial analysis

This section focuses on the methodology to produce the 'final water mask' based on spatial relationships. The two categories are first of all combined to obtain a segmentation result. The connected-component labeling algorithm is used to perform the segmentation to find regions of spatially connected pixels of the categories 'certainly and potentially water'. For each segmented region, if there is a spatial connection between both categories, this region may be labeled as surface water.

3. RESULTS AND ANALYSIS

We select images (Sentinel-2 data from Wuhan on Sep. 22, 2019, Shanghai on Mar. 10, 2018 and Guangzhou on Oct. 26, 2020) to test the performance of the SWM algorithm for a large spatial coverage. And, for a time series (6 Landsat

images and 3 Sentinel-2 images of July or Aug. between 2007 and 2021, and monthly Landsat images or Sentinel-2 images in 2020), we select image data around Nantan Lake to test the performance of long time-series dynamics. The locations and false-color images of these study areas can be found in Fig. 1.

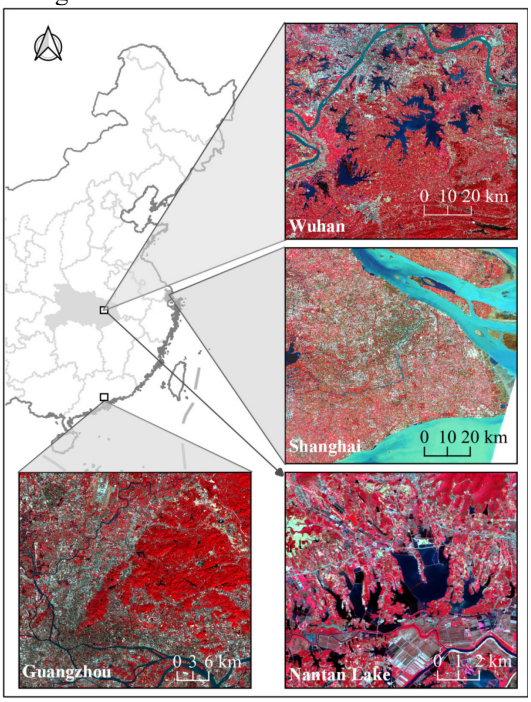

Fig. 1.Study areas and experimental data.

3.1. SWM results for large spatial coverages

To verify the proposed SWM algorithm, we analyze the performance of the proposed SWM algorithm in comparison to several water extraction methods (including supervised random forest classification method (RF) [7], hierarchical clustering method (HC) [8], multi-band threshold method (MBT) [9], and the Otsu method) for Wuhan, Shanghai, and Guangzhou. The SWM algorithm and Otsu method are based on the modified normalized difference water index (MNDWI). The evaluation sample points and ground truth images on each experimental data were set based on optical false-color images and Google Earth high-resolution images of the corresponding period.

The water extraction results are shown in Fig. 2, and the accuracy of the algorithm are reported in Table 1 using the overall accuracy (OA), F1 score (F1), producer's accuracy (PA), and user's accuracy (UA). We find that the proposed SWM algorithm can extract small water bodies more effectively and omission errors are reduced compared with these state-of-the-art algorithms. An average of approx. 97% (OA) and 0.95 (F1) is achieved. Overall, the SWM is found superior to other algorithms in terms of the integrity of the targeted water bodies especially in small-scale details, with less incorrect extractions, confirming the effectiveness of the algorithm.

Table 1 Water extraction accuracies for all the experimental areas in comparison to different classification methods

Study area	Method	OA (%)	PA (%)	UA (%)	F1
Shanghai	SWM	**95.87**	**93.50**	94.06	**0.9378**
	Otsu	92.20	77.90	**98.36**	0.8694
	HC	92.87	84.30	93.67	0.8874
	RF	92.43	83.00	93.57	0.8797
	MBT	93.73	87.80	93.01	0.9033
Wuhan	SWM	**97.23**	**93.20**	98.42	**0.9574**
	Otsu	88.53	71.70	92.16	0.8065
	HC	94.23	83.78	98.70	0.9063
	RF	92.57	78.70	98.75	0.8759
	MBT	94.03	83.10	**98.81**	0.9028
Guangzhou	SWM	**97.20**	**98.40**	93.54	**0.9591**
	Otsu	92.53	92.00	86.47	0.8915
	HC	86.73	60.20	**100.00**	0.7516
	RF	94.60	89.60	93.92	0.9171
	MBT	96.53	92.00	97.46	0.9465

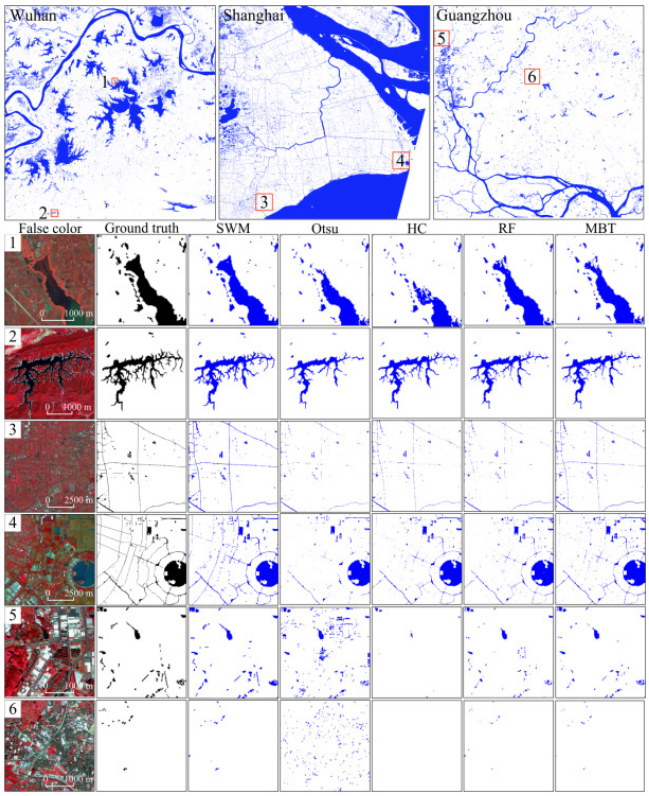

Fig. 2. The water extraction results using the proposed SWM method in comparison to other state-of-the-art algorithms.

3.2. SWM results of inter- and intra-year dynamics

In Fig. 3 we present the mapped trends of changes of the extracted water area from Nantan Lake. The results of the SWM extraction includes Landsat (circle) and Sentinel-2 (square) data; as reference, ground truth, and the Global Surface Water dataset developed by the European

Commission's Joint Research Centre (JRC) are presented. The deviation (ratio of the deviation value of the water area to the total water area in the experimental test regions is calculated from the ground truth) of different products is used to quantitatively measure the extraction accuracy. Three calibration points (2016, 2019, 2021) on the annual chart and five calibration points (Feb., Mar., Aug., Oct., Nov.) on the monthly chart are used to evaluate the stability of the SWM method for remote sensing images acquired by different satellite missions or sensors.

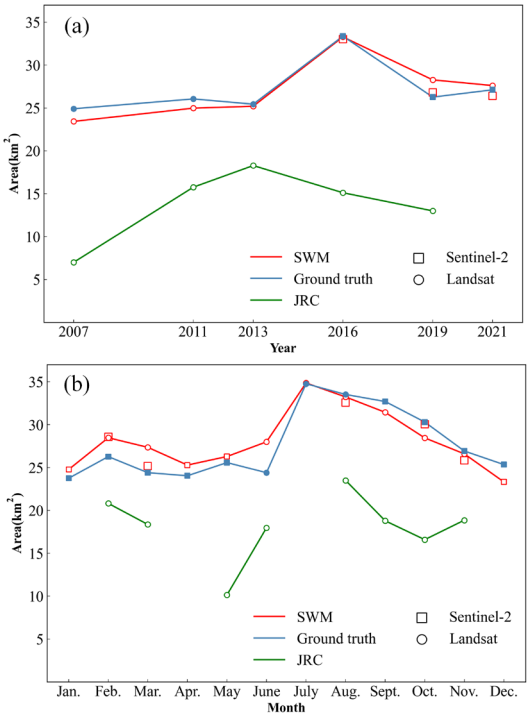

Fig. 3. The inter- and intra-year area changes of Nantan Lake extracted by SWM in comparison to ground truth and JRC products.

As shown in Fig. 3, the SWM results are close to the ground truth; in comparison, the results of the JRC are found to have comparatively large deviations. For annual results, the mean absolute deviations between the Landsat SWM results, Sentinels-2 SWM results, JRC products, and the ground truth are 3.5%, 1.9%, 49.0%, respectively; for monthly results, the numbers are 6.0%, 5.1%, 35.0%, respectively. The mean absolute deviations between the SWM results of Landsat and Sentinel-2 images at the calibration points are 3.6% and 3.9% for annual and monthly results, respectively. These results verify the effectiveness and accuracy of the SWM method applied to time-series optical images for automatic extraction of water bodies.

4. CONCLUSION

This study aims to solve two major problems of extracting small water bodies from optical remote sensing images: One is to develop a robust method to overcome the dilemma to reduce incorrect water extractions and at the same time increase the integrity of water extraction due to the spectral complexity of water and non-water objects. The other to provide a robust method that overcomes the challenge that lies in the spectral variability of the time-series optical images due to the temporal surface change or different calibration accuracy of different sensors. The proposed SWM approach develops a strategy to integrate the spatial information to make up for the indivisibility of spectral information of small water bodies. For the first time, the roughness of the water index is proposed to measure spatial variability of surface water and extract more complete small water bodies considering the large spatial variability of small water bodies and surrounding land cover categories.

5. ACKNOWLEDGEMENTS

This work was supported by National Natural Science Foundation of China under Grant No. 42171384.

6. REFERENCE

[1] J. Biggs, S. von Fumetti, and M. Kelly-Quinn, "The importance of small waterbodies for biodiversity and ecosystem services: implications for policy makers," *Hydrobiologia,* vol. 793, no. 1, pp. 3-39, Jun. 2017.

[2] H. Taubenböck, T. Esch, A. Felbier, M. Wiesner, A. Roth, and S. Dech, "Monitoring of mega cities from space," *Remote Sens. Environ.*, vol. 117, pp. 162-176, Feb. 2012.

[3] H. Taubenböck, M. Wurm, M. Netzband, H. Zwenzner, A. Roth, A. Rahmann, and S. Dech, "Flood risks in urbanized areas – Multi-sensoral approaches using remotely sensed data for risk management," *Nat. Hazards & Earth Sys. Sci.*, vol. 11, pp. 431-444, Feb. 2011.

[4] L. Li, H. Su, Q. Du, and T. Wu, "A novel surface water index using local background information for long term and large-scale Landsat images," *ISPRS J. Photogramm. Remote Sens.,* vol. 172, pp. 59-78, Feb. 2021.

[5] N. Otsu, "A Threshold Selection Method from Gray-Level Histograms," *IEEE Transactions on Systems, Man, and Cybernetics,* vol. 9, no. 1, pp. 62-66, Jan. 1979.

[6] I. Klein, U. Gessner, A. J. Dietz, and C. Kuenzer, "Global WaterPack – A 250 m resolution dataset revealing the daily dynamics of global inland water bodies," *Remote Sens. Environ.,* vol. 198, pp. 345-362, Sep. 2017.

[7] H. Chen, Q. Liang, Z. Liang, Y. Liu, and T. Ren, "Extraction of connected river networks from multi-temporal remote sensing imagery using a path tracking technique," *Remote Sens. Environ.,* vol. 246, Sep. 2020.

[8] M. C. R. Cordeiro, J.-M. Martinez, and S. Peña-Luque, "Automatic water detection from multidimensional hierarchical clustering for Sentinel-2 images and a comparison with Level 2A processors," *Remote Sens. Environ.,* vol. 253, Feb. 2021.

[9] F. Chen, X. Chen, T. Van de Voorde, D. Roberts, H. Jiang, and W. Xu, "Open water detection in urban environments using high spatial resolution remote sensing imagery," *Remote Sens. Environ.,* vol. 242, Jun. 2020.